RSC Advances

PAPER

View Article Online
View Journal | View Issue

Cite this: *RSC Adv.*, 2017, **7**, 24453

Facile synthesis of Fe_3O_4/MIL-101 nanocomposite as an efficient heterogeneous catalyst for degradation of pollutants in Fenton-like system

Chaocheng Zhao, *[ab] Pei Dong, [ab] Zongmei Liu,[ab] Guangrui Wu,[ab] Shuaijun Wang,[ab] Yongqiang Wang[ab] and Fang Liu[ab]

Received 15th February 2017
Accepted 27th April 2017

DOI: 10.1039/c7ra01883e

rsc.li/rsc-advances

An active Fe_3O_4/MIL-101 hybrid material was prepared *via* a simple *in situ* solvothermal method and characterized as a heterogeneous Fenton-like catalyst for Rhodamine B (RhB) degradation. The Fe_3O_4/MIL-101 exhibited enhanced catalytic performance for RhB degradation in a neutral solution. Under optimized conditions, almost 100% removal of 10 mg L^{-1} RhB was achieved in 30 min using 0.5 g L^{-1} Fe_3O_4/MIL-101 and 20 mM H_2O_2 at initial pH 7. The reusability of Fe_3O_4/MIL-101 was also investigated after four runs. On the basis of the characterization of the catalyst, the results of metal leaching, the effects of radical scavengers, and hydroxyl radical ($^{\bullet}OH$) determination, it was concluded that RhB is decomposed mainly by the attack of the hydroxyl radical ($^{\bullet}OH$), generated by the reaction of Fe^{2+} species with H_2O_2. MIL-101 showed a significant synergistic effect with Fe_3O_4, in which it played the role of a solid-acid catalyst with Lewis acid sites on its surface, ensuring that a Fenton-like reaction occurred in the neutral solution.

1. Introduction

The pollution of water resources by refractory organic compounds has become a serious environmental problem that has attracted much attention.[1] However, conventional wastewater treatment technology is not very effective for the degradation of refractory organic pollutants due to the stable structures of these organic compounds.[2,3] Among the available water remediation technologies, advanced oxidation processes (AOPs) are regarded as effective technologies for the degradation of hazardous organic pollutants in wastewater.[4] The Fenton oxidation process, one of the AOPs, seems to be promising due to its low cost and environmental benignity. However, in contrast with homogeneous Fenton oxidation, heterogeneous Fenton-like oxidation has received extensive attention, as it can overcome the drawbacks of homogeneous Fenton oxidation by working in mild conditions and producing almost no byproduct sludge after reaction.[5]

In recent years, metal–organic frameworks (MOFs) have attracted great attention because of their salient features, including a porous structure, extremely high surface area, tunable pore size, and functionality.[6–9] These unique properties endow MOFs with wide applications in the areas of catalysis,[10] molecular separations,[11] sensing,[12,13] and gas adsorption,[14] *etc.* Moreover, MOF materials also exhibit tremendous potential in the degradation of pollutants in the wastewater. For example, Jiang *et al.*[15] presented an approach to construct a photocatalytically active MOF as a catalyst for RhB degradation under visible light. Zhao *et al.*[16] reported that core–shell Fe_3O_4@MOFs could be used as a visible-light-driven catalyst for the degradation of dye pollutant with H_2O_2 as an electron acceptor. Jiang *et al.*[17] observed that MIL-53(Fe) could completely decompose RhB in the presence of H_2O_2 under visible light irradiation. Nevertheless, among all of them, the introduction of external energy is a vital factor to ensure their high catalytic activity, which will hamper their practical application caused by the large cost. To the best of our knowledge, excellent MOF-based Fenton-like catalyst without the aid of external energy has been rarely reported. Therefore, the goal of the present work is to provide a simply synthetic MOF-based Fenton-like catalyst which exhibits powerful efficiency for degradation of RhB without additional energy input and works in mild operation condition with wide application.

MIL-101(Fe) is a typical MOF material with an extremely large surface area and numerous transition metal sites.[18] Additionally, it has a zeotype crystal structure with high resistance to air, water and common solvents.[19] Therefore, MIL-101(Fe) was selected as the object of study in our research. Fe_3O_4 nanoparticles were used in the synthetic process and functionalized MIL-101(Fe) as a superparamagnetic model for degradation of RhB and magnetic recovery.

The proposed synthetic procedure involved *in situ* fabrication of MIL-101(Fe) in the presence of Fe_3O_4 nanoparticles, using a solvothermal method. The electrostatic interaction

[a]*College of Chemical Engineering, China University of Petroleum, Qingdao 266580, China. E-mail: zhaochch0821@163.com*

[b]*State Key Laboratory of Petroleum Pollution Control, Beijing 102206, China*

between Fe_3O_4 and metal ions induced chemical stabilization of magnetic nanoparticles. Thus, MOF crystals were uniformly enclosed by Fe_3O_4 to form a homogeneous magnetic product, identified as a Fe_3O_4/MIL-101. The physical and chemical characterization of Fe_3O_4/MIL-101 was conducted, and the applicability of this hybrid material in heterogeneous Fenton-like reaction was evaluated in view of the effect of the various processes, material stability, degradation mechanism, and the roles of Fe_3O_4 and MIL-101(Fe).

2. Materials and methods

2.1. Reagents and materials

Rhodamine B, *tert*-butanol and coumarin were obtained from Sigma-Aldrich, Taiwan. $FeCl_3 \cdot 6H_2O$, $FeCl_2 \cdot 4H_2O$ and terephthalic acid (H_2BDC) were purchased from Aladdin, China. The organic solvents used (*viz.*, ethanol, and dimethylformamide (DMF)) were obtained from Sinopharm, China. All reagents were of analytical grade without further purification.

2.2. Preparation of catalysts

First, Fe_3O_4 nanoparticles were synthesized *via* a chemical co-precipitation method.[20] Briefly, $FeCl_2 \cdot 4H_2O$ (2.0 g) and $FeCl_3 \cdot 6H_2O$ (5.2 g) were dissolved in 25 mL deionized water, followed by the addition of 0.85 mL concentrated hydrochloric acid. The resulting solution was added into a 500 mL three-necked round flask, and then 250 mL of NaOH solution (1.5 M) was dropwise into the above solution under vigorous non-magnetic agitation and N_2 protection at 80 °C. Afterwards, the obtained Fe_3O_4 suspension was aged for 30 min and cooled down to the room temperature. Finally, the black precipitate was isolated from the supernatant by magnetic decantation and washed with deionized water several times until the pH of the washings approached a neutral value.

For the preparation of Fe_3O_4/MIL-101, the freshly wet magnetic Fe_3O_4 particles (equal to 40 mg of dried Fe_3O_4) were dispersed in 20 mL of $FeCl_3 \cdot 6H_2O$ (2700 mg) DMF solution with ultrasonication for 10 min, and then in 40 mL of H_2BDC (824 mg) DMF solution with ultrasonication for another 30 min. The mixture was transferred into a Teflon-lined autoclave bomb and heated at 110 °C for 20 h. Thereafter, the brown solid was separated from the reaction medium with an external magnet, washed several times, and dried overnight in vacuum at 50 °C. The resulting product was identified as Fe_3O_4/MIL-101. MIL-101 was synthesized as in the above procedure without adding Fe_3O_4.

2.3. Catalyst characterization

The powder X-ray diffraction (XRD) patterns of samples were collected using a diffractometer (X'Pert Pro, Holland) with Cu Kα radiation (40 kV, 40 mA). The microscopic feature of the samples was observed using a transmission electron microscope (TEM) (JEM 2010, JEOL, Japan) operated at 200 kV. A Fourier Translation Infrared Spectroscopy (FT-IR) Spectrometer (Nicolet Nexus 670, America) was used to record the spectra of the samples in a range from 500 nm to 2500 nm. Nitrogen adsorption/desorption was analysed using a Micromeritics ASAP 2010 sorption analyser. The functional groups and the related oxidation state of the surface of the materials were analysed by X-ray photoelectron spectroscopy (XPS) on a PHI 5000 Versaprobe spectrometer equipped with a rotating Al anode generating Al Kα X-ray radiation at 1486.6 eV. The X-ray beam was monochromatized using seven crystals that were mounted on three Rowland circles. The zeta potentials of samples were measured by micro-electrophoresis apparatus (JS94J, Shanghai).

2.4. Experimental procedures

Batch trials were performed in glass beakers (150 mL) with mechanical stirring in the dark. The reaction suspension was prepared by adding the required amount of catalyst into 100 mL of a 10 mg L^{-1} RhB solution that had been adjusted to the desired pH value by H_2SO_4 or NaOH. The required amount of H_2O_2 was added to the solution to initiate the reaction. Then, the samples were extracted at set intervals using a 5 mL syringe and filtered immediately through a 0.22 μm filter film prior to analysis. To evaluate the contribution of homogeneous removal by the leaching ions, experiments were carried out as follows: after mixing Fe_3O_4/MIL-101 with deionized water (pH 7) for 30 min and removing the composite by filtering, the required amount of RhB was added into the filtrate. To test the stability of Fe_3O_4/MIL-101, the catalyst was gathered, washed, dried under vacuum, and reused in a fresh solution of RhB and H_2O_2 several times. All experiments were conducted in duplicate, and the relative error was less than 5%. Unless specifically noted, each experiment was carried out at an ambient temperature of 25 ± 1 °C and was exposed to air.

2.5. Sample analysis

The pH values were determined by a pH-meter (PHS-3C). The concentration of RhB was monitored at 554 nm with a dual-beam UV-visible spectrophotometer (TU-1901). The concentration of ferrous ions was measured colorimetrically with 1,10-phenanthroline at 510 nm on a UV/vis spectrophotometer (Lambda 25, PerkinElmer), as described previously.[21,22] $^{\bullet}OH$ produced in the Fenton-like system was estimated by employing coumarin (1.0 mM) as a selective trap for $^{\bullet}OH$. The fluorescence intensity of 7-hydroxycoumarin was determined by a fluorescence spectrophotometer (F97PRO, Lengguang Tech.) at $\lambda_{excitation} = 322$ nm and $\lambda_{emission} = 455$ nm.[23,24]

3. Results and discussion

3.1. Characterization of catalysts

In this study, Fe_3O_4/MIL-101 with different Fe_3O_4 loading amounts (*e.g.*, 40 mg, 80 mg, 120 mg, and 200 mg) were prepared for characterization and performance measurements. The smallest Fe_3O_4 loading amounts was determined to be 40 mg mainly because when any smaller loading amount of the composite was used, some free MIL-101 crystals remained in the solution even after a magnetic field was applied to the side wall of the vessel. Wide-angle XRD was used to identify the

crystalline phase of the samples. Fig. 1 shows the XRD pattern of Fe_3O_4, MIL-101 and Fe_3O_4/MIL-101 with the least amount of Fe_3O_4 (40 mg). The powder XRD patterns of MIL-101 were in accordance with the literature.[18] Five characteristic peaks for Fe_3O_4 and two characteristic peaks for MIL-101 were preserved in the pattern of Fe_3O_4/MIL-101, revealing that this hybrid material was composed of Fe_3O_4 and MIL-101.

Fig. 2 shows the morphologies of Fe_3O_4/MIL-101 with Fe_3O_4 loading amount of 40 mg. It is apparent from the SEM images (Fig. 2a) that MIL-101 exhibited a uniform size and the Fe_3O_4 nanoparticles attached to the external surface of the MIL-101 crystals were uniformly distributed, which is a result of the electrostatic interaction between the positively charged MIL-101 and negatively charged Fe_3O_4 (provided by the –OH on its surface). This interaction was supported by the zeta potentials of Fe_3O_4 and MOF.[25] Additionally, Fig. 2b illustrates that the nanoparticles possess a uniform polyhedral morphology. From a suitable perspective, MIL-101 presented a perfectly analogous hexagonal morphology in the TEM image, with many nanoparticles of Fe_3O_4 enclosing all loading amounts (Fig. 2c). The HRTEM image in Fig. 2d shows that the lattice fringe spacing of the nanoparticles was approximately 0.25 nm, which can be assigned to the (311) reflection of Fe_3O_4. More detailed information can be obtained from the TEM images (Fig. 3). The Fe_3O_4 particles were sparse when the loading amount was 40 mg, and the TEM images show clearly increasing Fe_3O_4 content on the surface of the hybrid material with increasing amounts of Fe_3O_4. This is consistent with the synthetic process with different loading amounts.

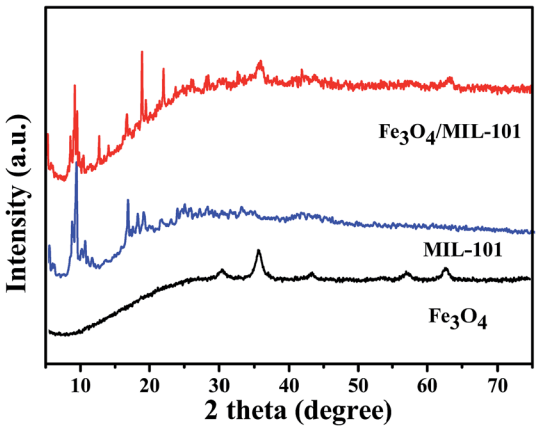

Fig. 1 XRD patterns of Fe_3O_4, MIL-101, and Fe_3O_4/MIL-101 with different Fe_3O_4 loading amounts of 40 mg, 80 mg, 120 mg and 200 mg.

Fig. 4 shows the FT-IR spectra of Fe_3O_4, MIL-101 and Fe_3O_4/MIL-101 with the least amount of Fe_3O_4 (40 mg). The FT-IR spectrum for Fe_3O_4 shows a typical band at 3415 cm^{-1}, which is attributed to O–H stretching vibrations. For MIL-101, the peak at 741 cm^{-1} is assigned to the out-of-plane bending vibration of C–H in the benzene ring of H_2BDC. The bands at 1681 and 1506 cm^{-1} are assigned to the asymmetric stretching

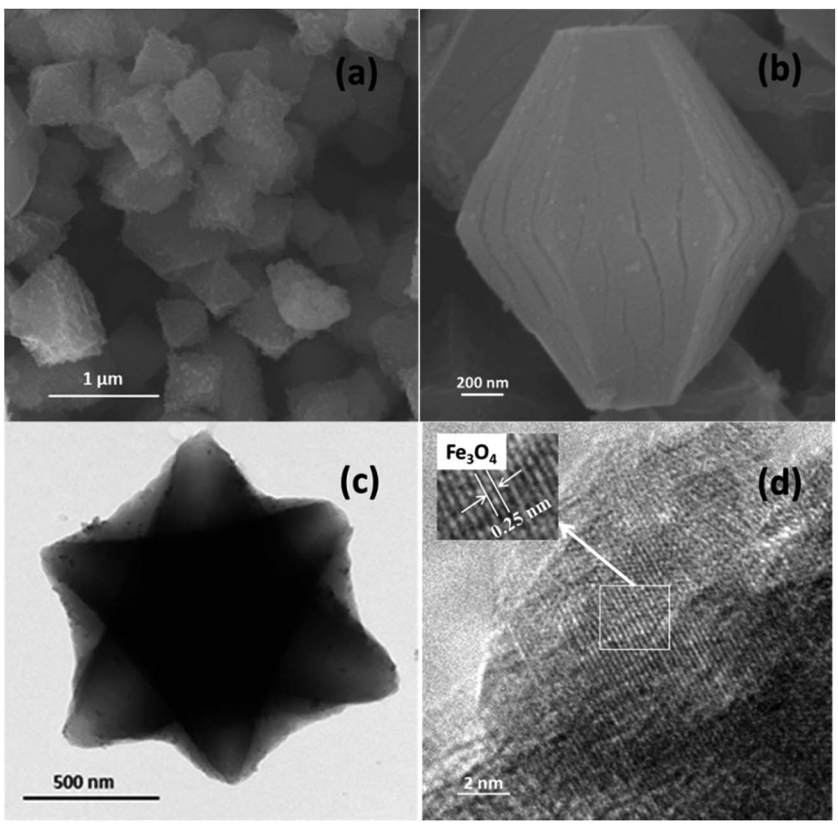

Fig. 2 Fe_3O_4/MIL-101 composite with Fe_3O_4 loading amount of 40 mg SEM images (a) and (b), TEM image (c) and HRTEM image (d).

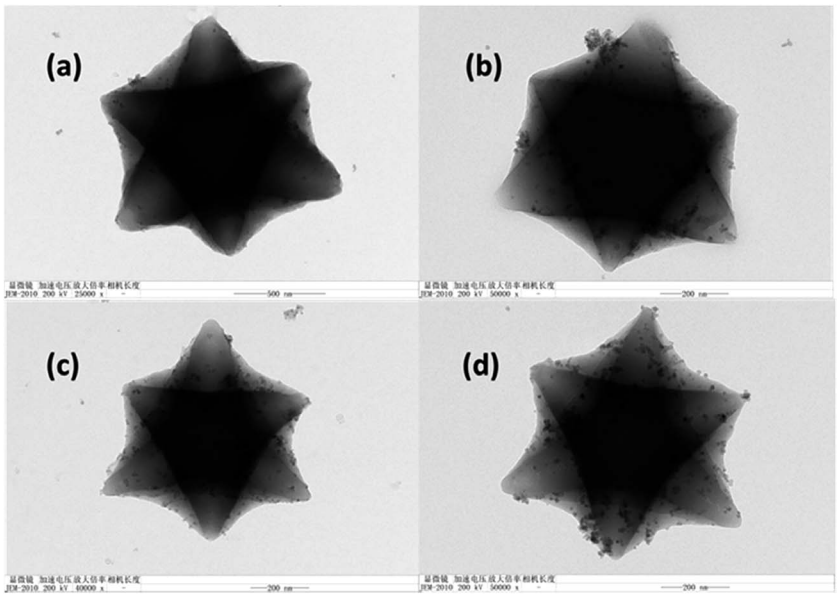

Fig. 3 TEM images of Fe_3O_4/MIL-101 composites with Fe_3O_4 loading amounts of 40 mg (a), 80 mg (b), 120 mg (c) and 200 mg (d).

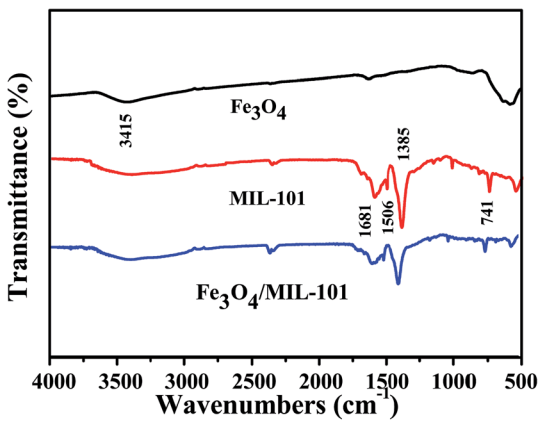

Fig. 4 FT-IR spectra of Fe_3O_4, MIL-101, and Fe_3O_4/MIL-101 with Fe_3O_4 loading amount of 40 mg.

of carboxyl groups in H_2BDC, whereas the band at 1385 cm^{-1} is assigned to the symmetric stretching of carboxyl groups in H_2BDC.[26] No special differences between MIL-101 and Fe_3O_4/MIL-101 were observed, and all the bands demonstrate the dominance of the properties of MIL-101 in the hybrid material.

The textural properties of samples were characterized by nitrogen adsorption isotherms. MIL-101 powder has an extremely high BET surface area and porous volume (1987.05 $m^2\ g^{-1}$ and 0.624 $cm^3\ g^{-1}$, respectively). Compared with MIL-101 powder, the surface area of Fe_3O_4/MIL-101 powder with Fe_3O_4 loading amounts of 40 mg was observed to be smaller by approximately 15.2% (Table 1). This may be due to the loading of Fe_3O_4 in the MIL-101 material as well as the activating role of the Fe(III) salt. On the other hand, the insignificant change in porosity of the Fe_3O_4/MIL-101 and MIL-101 could result from the small loading amount of Fe_3O_4, which ensures that Fe_3O_4/MIL-101 remains higher surface area and porous volume. The

Table 1 BET properties of Fe_3O_4/MIL-101

Sample	Fe_3O_4 (mg)	S_{BET} ($m^2\ g^{-1}$)	Pore size (nm)	Pore volume ($cm^3\ g^{-1}$)
MIL-101	0	1987.05	2.68	0.624
Fe_3O_4/MIL-101	40	1685.89	2.73	0.632

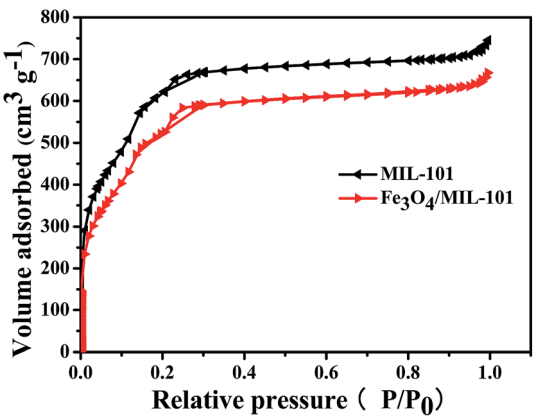

Fig. 5 Nitrogen adsorption–desorption isotherms for pure MIL-101 and Fe_3O_4/MIL-101 with Fe_3O_4 loading amount of 40 mg.

nitrogen adsorption–desorption isotherms exhibited a typical type-I form (Fig. 5), which indicates that the Fe_3O_4/MIL-101 composite has a typical microporous structure similar to that of pure MIL-101.

3.2. Catalytic activity of Fe_3O_4/MIL-101

Control experiments were conducted to compare the removal efficiencies at initial pH 7 with RhB concentration of 10 mg L^{-1}.

Fig. 6a shows the catalytic activity of Fe_3O_4/MIL-101 with different Fe_3O_4 loading amounts (40 mg, 80 mg, 120 mg and 200 mg). It is clearly seen that with decreasing Fe_3O_4 loading, the hybrid material showed gradual improvement in catalytic activity, indicating that MIL-101 crystals played a key role in the degradation of RhB. The high porosity and the presence of a large amount of oxygen groups on the MOF surfaces resulted in their high surface area and moderate polarity, thus facilitating effective interaction with RhB and accelerating the catalytic process. Fe_3O_4/MIL-101 with the least Fe_3O_4 loading amount of 40 mg provided the highest catalytic capacity. Therefore, it was employed in the following studies.

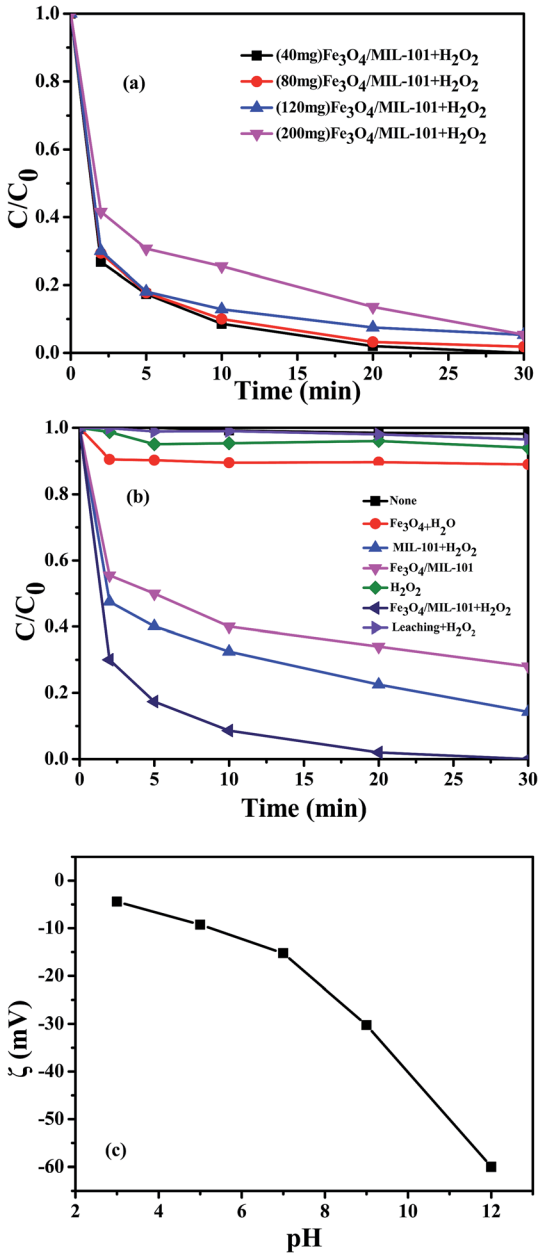

Fig. 6 (a) Removal of RhB with different loading amounts of Fe_3O_4 as catalysts at initial pH 7; (b) removal of RhB under different reaction conditions at initial pH 7; (c) the zeta potential of Fe_3O_4/MIL-101 at different pH values. Conditions: [catalyst] = 0.5 g L^{-1}, [RhB] = 10 mg L^{-1}, [H_2O_2] = 20 mM.

To clarify the excellent performance of Fe_3O_4/MIL-101, MIL-101 and Fe_3O_4 were also prepared and examined under same experimental conditions. As seen from Fig. 6b, no noticeable removal of RhB was observed in the presence of RhB alone. H_2O_2 only led to a slight removal of RhB within 30 min. In the leached metal–H_2O_2 system, the oxidation efficiency was greatly limited, with approximately 2% of RhB degraded after 30 min. This indicates that nearly all of reactions occur on the surface of catalyst, thus proving the stability of Fe_3O_4/MIL-10. In the presence of H_2O_2, the removal of RhB using Fe_3O_4/MIL-101 as the heterogeneous Fenton-like catalyst was notably higher than that for pure MIL-101 and Fe_3O_4, implying that the catalytic activity was enhanced by the introduction of MIL-101 and Fe_3O_4. There is a synergistic effect in the hybrid material, which enhances the relative rates of mass transfer to reactive sites and subsequent chemical reaction at the reactive sites. With 0.5 g L^{-1} Fe_3O_4/MIL-101 only, approximately 65% removal was observed, mainly due to surface adsorption of Fe_3O_4/MIL-101. Furthermore, the effect of surface adsorption was investigated. The adsorption of RhB is sensitive with surface charge of Fe_3O_4/MIL-101. Therefore, the zeta potential of Fe_3O_4/MIL-101 was provided to better understand the adsorption behavior of RhB in solution. As seen from Fig. 6c, the absolute values of zeta potential increased obviously with the increase of initial pH, which indicates that Fe_3O_4/MIL-101 has negative charge in solution at initial pH 3, 5, 7, 9 and 12, and the negative charges of Fe_3O_4/MIL-101 particles increase with the increase of pH. As we know, RhB is a kind of cationic dyes. Thus, there are electrostatic interaction between Fe_3O_4/MIL-101 with negative charge and RhB molecule with positive charge, and the adsorption properties of Fe_3O_4/MIL-101 increased gradually with the increase of zeta potential. Several experiments were performed to explore the interaction between catalysis and adsorption. Desorption was almost completely achieved *via* ultrasonic treatment of the used hybrid material for 30 min with using ethanol as solvent. The result was confirmed by desorbing RhB from Fe_3O_4/MIL-101 after the surface adsorption reaction, resulting in nearly 100% desorption. However, after the recovery of used Fe_3O_4/MIL-101 from the Fenton-like system, RhB desorption percentage was only approximately 14% in the same experiment conditions. All surface adsorption–desorption experiments demonstrate that Fe_3O_4/MIL-101 has a strong adsorption property. However, in the presence of H_2O_2, catalytic action plays an absolutely leading role rather than adsorption. Also, it is speculated that the adsorption action of Fe_3O_4/MIL-101 may facilitate the process of catalysis.

3.3. Effect of pH

It is well-known that the performance of the Fenton reaction is strongly correlated to the solution pH.[27,28] Therefore, the effect of the initial pH value on the degradation of RhB with Fe_3O_4/MIL-101 catalyst was determined as presented in Fig. 7. Approximately 65% and 63% of RhB were removed after 30 min of reaction at initial pH 3 and 12, respectively. The amount

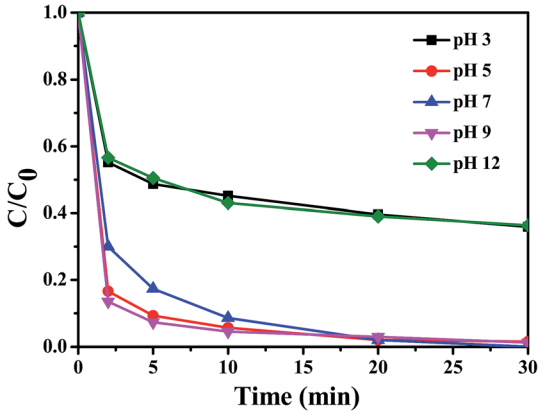

Fig. 7 Influence of initial pH on the degradation of RhB in the Fe_3O_4/MIL-101-H_2O_2 system. Conditions: [Fe_3O_4/MIL-101] = 0.5 g L^{-1}, [RhB] = 10 mg L^{-1}, [H_2O_2] = 20 mM.

removed increased dramatically, reaching almost 100% at initial pH 5, 7, and 9. Thus, the effect of initial pH on the degradation of phenol is clear. The removal rate achieved highest efficiency when the initial RhB solution had a nearly neutral pH. In contrast to the general Fenton reaction activated in an acidic environment, Fe_3O_4/MIL-101 shows extraordinary performance as an efficient Fenton-like heterogeneous catalyst in a steerable neutral solution of the pollutant, which is a great advantage for improve efficiency and cost saving. This may be related to the function of solid-acid catalyst of the MIL-101, which will be introduced in detail below. On the other hand, the amount removed decreased dramatically at initial pH 3 and 12, which is reasonable because compared to neutral environments, MOF materials lack stability in acidic and alkaline conditions, thus hindering the process of catalysis.

3.4. Stability of Fe_3O_4/MIL-101

The stability of the catalyst was evaluated by reusing it in four successive experiments under same reaction conditions. When the initial solution pH was 7, approximately 60% of RhB could still be removed in the fourth run after 30 min (data not shown). Additionally, as seen from Fig. 8a, nearly 100% RhB was further removed in each cycle if the reaction time was extended to 60 min, indicating the good stability and long lifetime of the composite. The concentration of dissolved Fe in the solution was investigated during the Fenton-like oxidation of RhB (Fig. 8b). The concentration of ferrous ion increased and reached a maximum of approximately 9 μg L^{-1} at 30 min, when almost complete removal of RhB occurred. Following this, the Fe^{2+} concentration decreased to approximately 2 μg L^{-1} at 60 min, similar to the results reported in earlier studies.[29,30] In the ascending interval, oxidation of the catalyst by H_2O_2 may have released ferrous ions into solution, generating $^{\cdot}OH$. After RhB was almost completely removed, the decrease in concentration probably resulted from the oxidation of the dissolved ferrous ions to ferric ions by the remaining oxidants.[31] Thus, the increase of total dissolved iron may be a result of the leaching of ferrous and ferric ions from Fe_3O_4/MIL-101, as well as the

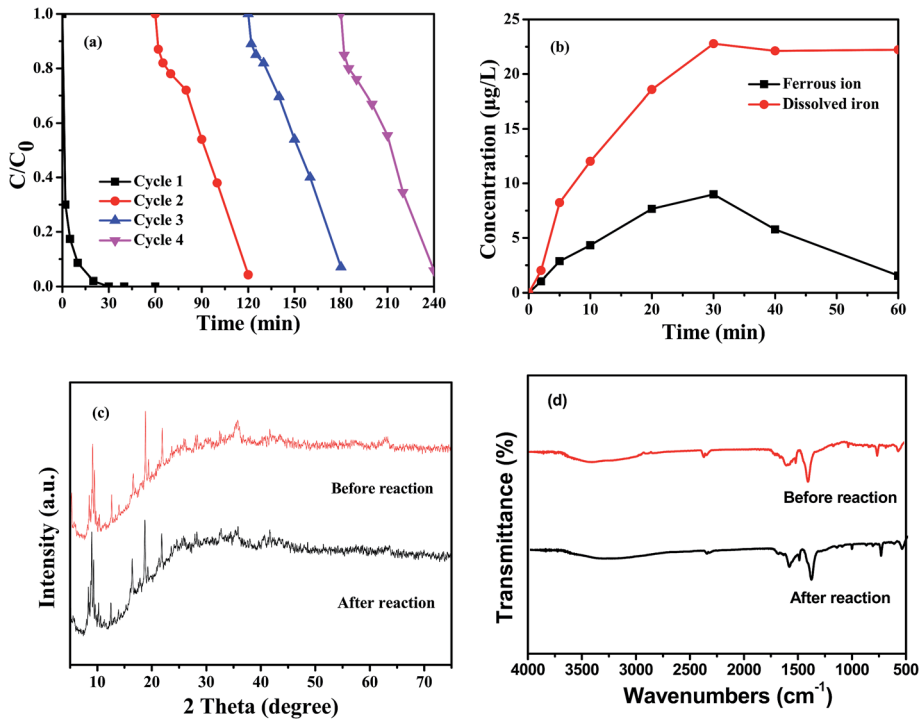

Fig. 8 (a) Catalytic property of Fe_3O_4/MIL-101 during repeated use at neutral conditions; (b) variation of the concentration of dissolved iron and ferrous ion in solution during RhB degradation; (c) XRD patterns of the Fe_3O_4/MIL-101 before and after Fenton-like reaction; (d) FT-IR spectra of the Fe_3O_4/MIL-101 before and after Fenton-like reaction. Conditions: [Fe_3O_4/MIL-101] = 0.5 g L^{-1}, [RhB] = 10 mg L^{-1}, [H_2O_2] = 20 mM, initial pH 7.

oxidation of ferrous ions in solution. The loss of iron amounted to 22.2 μg L^{-1}, negligible compared with the 0.5 g L^{-1} of catalyst used. To further check the structural stability of the catalyst, the phase structure and molecular structure of the Fe_3O_4/MIL-101 after four times of repeated use were recorded by XRD (Fig. 8c) and FT-IR spectra (Fig. 8d). The almost identical XRD patterns and FT-IR spectra before and after the Fenton-like reactions illustrates that the chemical and crystal structure of the catalyst are almost unchanged after four repeated reactions. These results demonstrate the high long-term stability of our Fe_3O_4/MIL-101 Fenton-like catalyst.

3.5. Mechanistic study

It is well-known that *tert*-butanol (TBA) is mainly used as a quenching agent for ˙OH because of its high reactivity ($k_{\cdot OH}$: 3.8–7.6 × 10^8 M^{-1} s^{-1}).[32–34] The actual reactive specie mediating the process was identified by determining the influence of TBA as a radical scavenger on the degradation of RhB, as shown in Fig. 9a. When no quenching agent was added, approximately 100% RhB was degraded in 30 min. The addition of 100 mM TBA resulted in the decrease of RhB removal (in 30 min) to 95%, with almost no inhibition, because of a small amount of added radical scavenger. However, the amount removed decreased dramatically, reaching only 15%, with 1000 mM TBA. Thereafter, there was a second apparent jump when the added TBA was approximately 2000 mM, with nearly 100% inhibition. Reasonably, the inhibition was enhanced with the increase in the concentration of TBA, indicating that ˙OH radicals were involved in the oxidation process. Moreover, excess TBA in solution not only scavenged all the produced ˙OH but also resulted in competitive adsorption against RhB due to the interaction of functional groups between TBA and Fe_3O_4/MIL-10, so that the inhibition effect reached almost 100%.

The results of the radical scavenger experiments are validated by the fluorescence spectra in Fig. 9b. We observed that in the Fe_3O_4/MIL-101–H_2O_2–coumarin system, the oxidation of coumarin by the generated ˙OH radicals resulted in a rapid increase of the fluorescence intensity of the product 7-hydroxycoumarin with increasing reaction time. Coumarin did not easily react with H_2O_2 in the absence of the catalyst. The fluorescence intensity in the system gradually increased, indicating that H_2O_2 activated by Fe_3O_4/MIL-101 produced strong oxidizing ˙OH radical in the Fenton-like system.

The Lewis acid catalytic properties of MOFs have already been demonstrated for many reactions, including cyanosilylation of carbonyl compounds,[35] epoxide methanolysis,[36] isomerizations of α-pinene oxide and citronella,[37] alkene cyclopropanation,[38] *etc.* The Fe_3O_4/MIL-101 fabricated in this study also has a solid-acid catalytic property, which stems from the creation of a coordination vacancy upon unsaturated coordination of Fe ions in the MIL-101 structure. To better understand the interaction between the Lewis acid character and the neutral reaction environment, the change of solution pH value was monitored as a function of time at different initial pH (Fig. 9c). Obviously, the pH values remained unchanged after 5 min at approximately 3.8, 4.1, and 4.2 when the initial pH values were 5, 7, and 9,

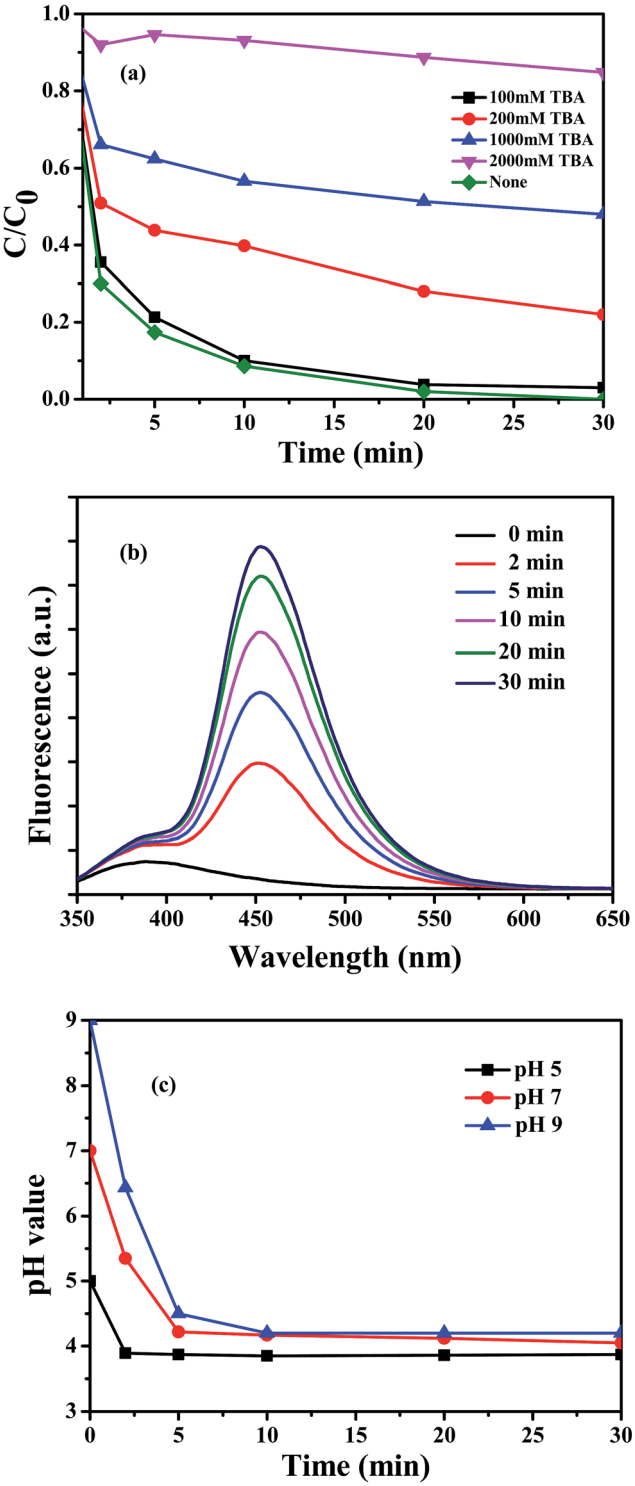

Fig. 9 (a) Effects of TBA on the degradation of RhB at initial pH 7; (b) fluorescence intensity of 7-hydroxycoumarin produced in the Fenton-like reaction at initial pH 7; (c) pH variation during the reaction in the Fe_3O_4/MIL-101–H_2O_2 system at different initial pH. Conditions: [Fe_3O_4/MIL-101] = 0.5 g L^{-1}, [RhB] = 10 mg L^{-1}, [H_2O_2] = 20 mM.

respectively. The change of pH values was probably due to the effect of the Lewis acid sites in the structure of MIL-101, in which the incompletely coordinated Fe ions could coordinate

with H_2O and supply H^+ in the initially neutral Fenton-like system, as shown in eqn (1).

On the basis of the above information, a possible reaction mechanism for H_2O_2 activated by Fe_3O_4/MIL-101 under neutral conditions is proposed in Fig. 10. First of all, the Lewis acid sites in the structure of the MIL-101 provide H^+ in initially neutral aqueous solution (eqn (1)). As reported by other researchers,[39–41] the initially generated Fe^{2+} species can react with H_2O_2 to generate $^{\cdot}OH$ (eqn (2)), where Fe^{2+} stands for Fe(II) sites on the catalyst surface. Additional Fe^{2+} species are produced through the reactions of the formed Fe^{3+} species with H_2O_2 (eqn (3)) and $HO_2^{\cdot}$ (eqn (4)). This is further accompanied by competitive reactions that can negatively affect the oxidation process, as shown in eqn (5)–(10). Finally, RhB is broken down, mainly by hydroxyl radical on the surface of catalyst (eqn (11)). It is worth mentioning that all the reactions occur on the surface of the catalyst, in accordance with the result of the leaching experiment, as shown in Fig. 6b.

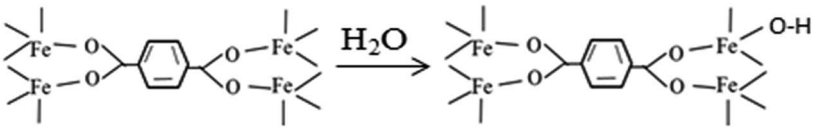

(1)

$$\equiv Fe^{2+} + H_2O_2 + H^+ \rightarrow \equiv Fe^{3+} + {}^{\cdot}OH + H_2O \quad (2)$$

$$\equiv Fe^{3+} + H_2O_2 \rightarrow \equiv Fe^{2+} + HO_2^{\cdot} + H^+ \quad (3)$$

$$\equiv Fe^{3+} + HO_2^{\cdot} \rightarrow \equiv Fe^{2+} + O_2 + H^+ \quad (4)$$

$$^{\cdot}OH + Fe^{2+} \rightarrow OH^- + Fe^{3+} \quad (5)$$

$$^{\cdot}OH + H_2O_2 \rightarrow H_2O + HO_2^{\cdot} \quad (6)$$

$$Fe^{2+} + HO_2^{\cdot} \rightarrow Fe^{3+} + HOO^- \quad (7)$$

$$HO_2^{\cdot} + HO_2^{\cdot} \rightarrow H_2O_2 + O_2 \quad (8)$$

$$^{\cdot}OH + HO_2^{\cdot}(O_2^{\cdot -}) \rightarrow O_2 + H_2O(+OH^-) \quad (9)$$

$$^{\cdot}OH + {}^{\cdot}OH \rightarrow H_2O_2 \quad (10)$$

$$^{\cdot}OH + RhB \rightarrow \text{degraded products} \quad (11)$$

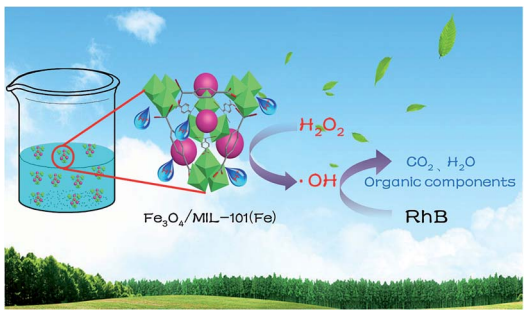

Fig. 10 Mechanisms for RhB degradation by Fe_3O_4MIL-101–H_2O_2 system.

4. Conclusions

In this study, Fe_3O_4/MIL-101 was successfully synthesized *via* a simple solvothermal process and found to be highly efficient and environmentally benign for the heterogeneous activation of H_2O_2 in Fenton-like system without additional energy input. The prepared Fe_3O_4/MIL-101 exhibited enhanced catalytic performance for degradation of RhB in a neutral Fenton-like solution, which was superior to those of pure Fe_3O_4 and MIL-101. This enhancement of the catalytic performance has been demonstrated due to the significant synergistic effect between Fe_3O_4 and MIL-101, in which MIL-101 played the role of a solid-acid catalyst with Lewis acid sites on its surface. Compared with the traditional Fenton systems which work under strongly acidic environment, the neutral operation condition of Fe_3O_4/MIL-101 is more suitable for practical water treatment. The as-prepared Fe_3O_4/MIL-101 sample exhibited magnetic property for easy separation and high long-term stability on the degradation of the organic pollutants. The results from this study shed light on the application of MOF-based solid-acid catalyst in environmental remediation field with mild conditions and low-energy treatment.

Acknowledgements

This work was supported by the National Science and Technology Major Project (No. 2016ZX05040003); and the Postgraduate Innovation Project of China University of Petroleum (No. YCXJ2016035).

References

1 Z. Ma, X. Wei, S. Xing and J. Li, *Catal. Commun.*, 2015, **67**, 68–71.
2 O. A. Yildirim, H. Arslan and S. Sönmezoğlu, *Appl. Surf. Sci.*, 2016, **390**, 111–121.

3 B. Li, Y. Zhang, X. Zhou, Z. Liu, Q. Liu and X. Li, *J. Alloys Compd.*, 2016, **673**, 265–271.
4 W. Liu, C. Fang, Y. Huang, L. Ai, F. Yang, Z. Wang and J. Liu, *RSC Adv.*, 2016, **6**, 93558–93563.
5 J. Fang, X. Huang, Q. Zhang, J. Chen and X. Wang, *Appl. Surf. Sci.*, 2016, **360**, 994–998.
6 Q.-L. Zhu and Q. Xu, *Chem. Soc. Rev.*, 2014, **43**, 5468–5512.
7 M. Drobek, J.-H. Kim, M. Bechelany, C. Vallicari, A. Julbe and S. S. Kim, *ACS Appl. Mater. Interfaces*, 2016, **8**, 8323–8328.
8 S. Zhang, Z. Jiao and W. Yao, *J. Chromatogr. A*, 2014, **1371**, 74–81.
9 X. Zhang, B. Li, H. Ma, L. Zhang and H. Zhao, *ACS Appl. Mater. Interfaces*, 2016, **8**, 17389–17394.
10 M. Zhao, K. Deng, L. He, Y. Liu, G. Li, H. Zhao and Z. Tang, *J. Am. Chem. Soc.*, 2014, **136**, 1738–1741.
11 A. Kertik, A. L. Khan and I. F. J. Vankelecom, *RSC Adv.*, 2016, **6**, 114505–114512.
12 X.-L. Huang, L. Liu, M.-L. Gao and Z.-B. Han, *RSC Adv.*, 2016, **6**, 87945–87949.
13 J. A. Gustafson and C. E. Wilmer, *J. Phys. Chem. C*, 2017, **121**, 6033–6038.
14 F. Rezaei, S. Lawson, H. Hosseini, H. Thakkar, A. Hajari, S. Monjezi and A. A. Rownaghi, *Chem. Eng. J.*, 2017, **313**, 1346–1353.
15 C. Zhang, L. Ai and J. Jiang, *J. Mater. Chem. A*, 2015, **3**, 3074–3081.
16 H. Zhao, L. Qian, H. Lv, Y. Wang and G. Zhao, *ChemCatChem*, 2015, **7**, 4148–4155.
17 L. Ai, C. Zhang, L. Li and J. Jiang, *Appl. Catal., B*, 2014, **148–149**, 191–200.
18 I. Y. Skobelev, A. B. Sorokin, K. A. Kovalenko, V. P. Fedin and O. A. Kholdeeva, *J. Catal.*, 2013, **298**, 61–69.
19 G. Férey, C. Mellot-Draznieks, C. Serre, F. Millange, J. Dutour, S. Surblé and I. Margiolaki, *Science*, 2005, **309**, 2040–2042.
20 M. H. Mashhadizadeh, M. Amoli-Diva and K. Pourghazi, *J. Chromatogr. A*, 2013, **1320**, 17–26.
21 C. Lee, C. R. Keenan and D. L. Sedlak, *Environ. Sci. Technol.*, 2008, **42**, 4921–4926.
22 A. L.-T. Pham, C. Lee, F. M. Doyle and D. L. Sedlak, *Environ. Sci. Technol.*, 2009, **43**, 8930–8935.
23 P. Hu, Y. Liu, B. Jiang, X. Zheng, J. Zheng and M. Wu, *Ind. Eng. Chem. Res.*, 2015, **54**, 8277–8286.
24 K.-i. Ishibashi, A. Fujishima, T. Watanabe and K. Hashimoto, *Electrochem. Commun.*, 2000, **2**, 207–210.
25 S.-H. Huo and X.-P. Yan, *Analyst*, 2012, **137**, 3445–3451.
26 S. Zhang, Z. Du and G. Li, *Talanta*, 2013, **115**, 32–39.
27 Z. Wan and J. Wang, *RSC Adv.*, 2016, **6**, 103523–103531.
28 W. Wang, M. Zhou, Q. Mao, J. Yue and X. Wang, *Catal. Commun.*, 2010, **11**, 937–941.
29 L. Xu and J. Wang, *Environ. Sci. Technol.*, 2012, **46**, 10145–10153.
30 J. Feng, X. Hu and P. L. Yue, *Environ. Sci. Technol.*, 2004, **38**, 5773–5778.
31 M. Luo, D. Bowden and P. Brimblecombe, *Appl. Catal., B*, 2009, **85**, 201–206.
32 Y. Yao, Y. Cai, G. Wu, F. Wei, X. Li, H. Chen and S. Wang, *J. Hazard. Mater.*, 2015, **296**, 128–137.
33 M. Li, D. Wen, Z. Qiang and J. Kiwi, *RSC Adv.*, 2017, **7**, 7640–7647.
34 T. Zhang, H. Zhu and J.-P. Croue, *Environ. Sci. Technol.*, 2013, **47**, 2784–2791.
35 M. Fujita, Y. J. Kwon, S. Washizu and K. Ogura, *J. Am. Chem. Soc.*, 1994, **116**, 1151–1152.
36 L. H. Wee, M. R. Lohe, N. Janssens, S. Kaskel and J. A. Martens, *J. Mater. Chem.*, 2012, **22**, 13742–13746.
37 L. Alaerts, E. Seguin, H. Poelman, F. Thibault-Starzyk, P. A. Jacobs and D. E. De Vos, *Chem.–Eur. J.*, 2006, **12**, 7353–7363.
38 A. Corma, H. García and F. X. Llabrés i Xamena, *Chem. Rev.*, 2010, **110**, 4606–4655.
39 R. C. C. Costa, F. C. C. Moura, J. D. Ardisson, J. D. Fabris and R. M. Lago, *Appl. Catal., B*, 2008, **83**, 131–139.
40 W. Luo, L. Zhu, N. Wang, H. Tang, M. Cao and Y. She, *Environ. Sci. Technol.*, 2010, **44**, 1786–1791.
41 X. Hu, B. Liu, Y. Deng, H. Chen, S. Luo, C. Sun, P. Yang and S. Yang, *Appl. Catal., B*, 2011, **107**, 274–283.